Imaging Science in Dentistry 2021; 51: 107-15
https://doi.org/10.5624/isd.20200259

Photoacoustic imaging of occlusal incipient caries in the visible and near-infrared range

Evair Josino da Silva[1], Erica Muniz de Miranda[2], Cláudia Cristina Brainer de Oliveira Mota[3], Avishek Das[2,*], Anderson Stevens Leônidas Gomes[1,2]

[1]*Graduate Program in Dentistry, Universidade Federal de Pernambuco, Recife, Brazil*
[2]*Department of Physics, Universidade Federal de Pernambuco, Recife, Brazil*
[3]*Faculty of Dentistry, Centro Universitário Tabosa de Almeida, Caruaru, Brazil*

ABSTRACT

Purpose: This study aimed to demonstrate the presence of dental caries through a photoacoustic imaging system with visible and near-infrared wavelengths, highlighting the differences between the 2 spectral regions. The depth at which carious tissue could be detected was also verified.

Materials and Methods: Fifteen permanent molars were selected and classified as being sound or having incipient or advanced caries by visual inspection, radiography, and optical coherence tomography analysis prior to photoacoustic scanning. A photoacoustic imaging system operating with a nanosecond pulsed laser as the light excitation source at either 532 nm or 1064 nm and an acoustic transducer at 5 MHz was developed, characterized, and used. En-face and lateral (depth) photoacoustic signals were detected.

Results: The results confirmed the potential of the photoacoustic method to detect caries. At both wavelengths, photoacoustic imaging effectively detected incipient and advanced caries. The reconstructed photoacoustic images confirmed that a higher intensity of the photoacoustic signal could be observed in regions with lesions, while sound surfaces showed much less photoacoustic signal. Photoacoustic signals at depths up to 4 mm at both 532 nm and 1064 nm were measured.

Conclusion: The results presented here are promising and corroborate that photoacoustic imaging can be applied as a diagnostic tool in caries research. New studies should focus on developing a clinical model of photoacoustic imaging applications in dentistry, including soft tissues. The use of inexpensive light-emitting diodes together with a miniaturized detector will make photoacoustic imaging systems more flexible, user-friendly, and technologically viable. ***(Imaging Sci Dent 2021; 51: 107-15)***

KEY WORDS: Diagnostic Imaging; Dental Caries; Photoacoustic Techniques; Tomography, Optical Coherence

Introduction

Dental caries causes irreversible progressive demineralization in teeth, both in enamel and dentin. Caries grow silently until changes in enamel become clinically visible. If left unchecked, tissue destruction is inevitable.[1] Therefore, early caries detection is important, since it enables preventive strategies and conservative procedures to be performed to control the disease.[2,3] Traditionally, caries are diagnosed through visual inspection and dental radiographs are complementarily employed. However, visual inspection is a subjective method in which the professional's experience directly influences the diagnosis, and a certain level of demineralization is necessary for tissue to be visible on a radiograph.[4,5] Due to these limitations, the last few years have seen an increased interest in the development of new methods of caries diagnosis with highly accurate and non-invasive methods, such as transillumination, fluorescence-based imaging, optical coherence tomography (OCT), and photoacoustic (PA) imaging.[6-13]

In the early 1880s, Bell,[14,15] Tyndall,[16] and Röntgen[17] in-

This study was supported by FACEPE/CNPQ and INCT-INFO (465.763/2014-6).
Received September 21, 2020; Revised November 27, 2020; Accepted December 8, 2020
*Correspondence to : Dr. Avishek Das
Department of Physics, Universidade Federal de Pernambuco, Recife, 50670-901, Pernambuco, Brazil
Tel) 55-81-99397-8338, E-mail) avishek55das@gmail.com

Imaging Science in Dentistry · pISSN 2233-7822 eISSN 2233-7830

dependently discovered what is now known as the PA effect. Bell found that materials can emit sound waves when illuminated by modulated light, identified that the intensity of the emitted sound was wavelength-dependent, and therefore attributed the phenomenon to an optical absorption process. In 1977, Hordvik and Schlossberg[18] used the PA technique to measure the absorption coefficient in solid samples with high sensitivity. Since then, PA has been exploited in a myriad of applications, leading to PA sensing, PA spectroscopy, and PA tomography or PA imaging as methods to image materials and biomaterials in a noninvasive way.[19-23] As pointed out by Li et al.,[22] PA tomography can cover a wide range of dimensions of interest for image generation, with spatial resolution ranging from hundreds of nanometers to 1 mm, and penetration depths from 10 μm to 10 cm. Furthermore, their study reported imaging results in biological tissues ranging from cells to human organs.[22]

In dentistry, PA methods have been demonstrated in studies of caries diagnostics,[13,24-27] periodontology,[28,29] dental implants,[30] and blood detection in dental pulp.[31] Given the potential of this method as a noninvasive imaging technique, its applications in dentistry are still in the initial stages, with pioneer work dating from 2006.[24] This fact led us to develop the work reported here, aiming to stimulate further studies of dental caries detection using PA imaging.

The purpose of this study was to examine the presence of incipient and advanced caries through a PA imaging system with visible and near-infrared wavelengths. After developing the PA imaging system, 2 different wavelengths were employed (532 nm and 1064 nm) as the linear absorption differs as the wavelength changes.

Materials and Methods

This experimental laboratory study was carried out after receiving approval from the Ethics Committee on Humans Research (process number 2.989.712) of Universidade Federal de Pernambuco, Pernambuco, Brazil, in accordance with the Helsinki Declaration.

Sample preparation

Fifteen permanent molar teeth were obtained from a tooth bank (Centro Universitário Tabosa de Almeida, Caruaru, Pernambuco, Brazil), analyzed by visual inspection, and divided into 3 groups as follows: 5 sound teeth; 5 teeth with incipient caries, representing the beginning of the pathological process but still without cavitation; and 5 teeth with advanced caries, representing the stage with evident dentin involvement. The sample characterization criteria employed followed the International Caries Detection and Assessment System categorization.[32]

The teeth had their root portion included with colorless self-curing acrylic resin (Jet Clássico, São Paulo, Brazil) in a matrix with the occlusal surface parallel to the ground, in order to standardize the sample positioning during PA imaging and OCT scanning. The samples were then kept in deionized water under refrigeration until the end of the experiment to avoid cracks and fractures.

Radiography and OCT

The teeth were evaluated by digital radiography, taken using a Focus intraoral X-ray machine (Instrumentarium Dental, Tuusula, Finland), with settings of 70 kV and 7 mA, using a photostimulable phosphor (PSP) plate and a focus-film distance of 30 cm. The exposure time was 0.3 s, as determined based on a previous pilot study. The sensor was read by a digital system Digora Optime scanner (Soredex, Helsinki, Finland), and an image was generated for each tooth on the PSP plate using the CLINIVIEW software (Instrumentarium Dental, Tuusula, Finland).

The teeth were also scanned by OCT, an imaging technique based on the backscattering and reflective properties of incident light on samples that provides depth information for the structures under analysis.[10,12,33,34]

For this experiment, 2 commercial OCT systems were utilized, both operating in the spectral domain. To obtain cross-sectional 2-dimensional (2D) images, an OQ LabScope (Lumedica, Durham, NC, USA) was employed, using a light source with a central wavelength of 840 nm and a depth resolution of 7 μm in air and 5 μm in tissue, generating an image with a size of 512 × 512 pixels. To obtain volumetric 3-dimensional (3D) images, a Ganymede OCT (Thorlabs Inc., Newton, NJ, USA) was employed, using a super-luminescent diode as a light source, with a central wavelength of 930 nm, a spectral bandwidth of 100 nm, a maximum output power of 5 mW, and an axial resolution of 5 μm. The axial resolution determined the spatial resolution of the measured biostructure.

Cross-sectional 2D and volumetric 3D images were obtained from the occlusal surface of teeth, aiming to verify the presence of incipient caries, as seen in the PA images. For both 2D and 3D scanning, the samples were positioned perpendicular to the beam light in both systems. The analysis was performed along the region of interest (ROI) of the occlusal surface, to identify the presence or absence of demineralization.

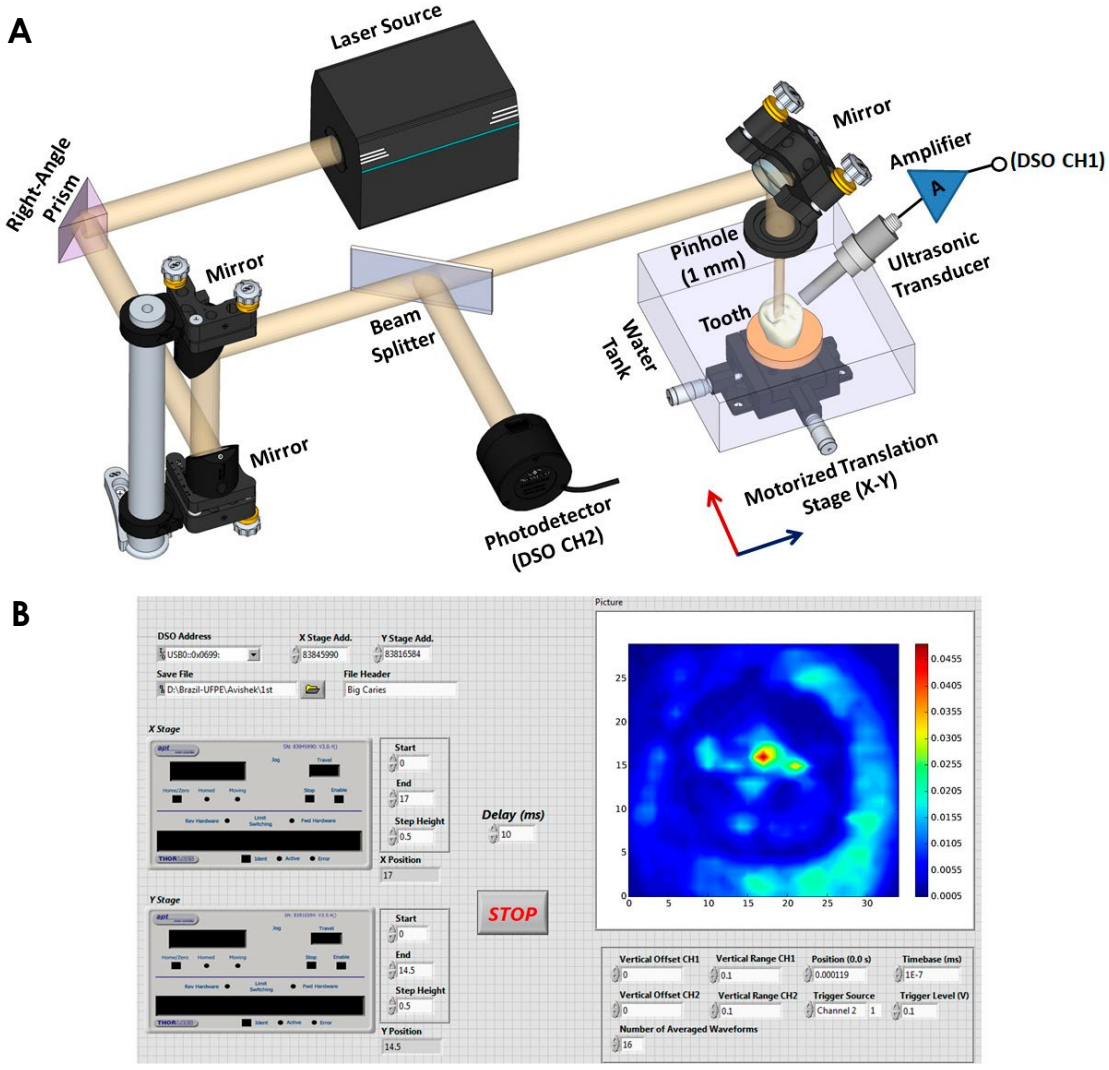

Fig. 1. A. Schematic diagram of the lab-made photoacoustic imaging system. B. Data acquisition and image reconstruction program in LabVIEW.

PA imaging system and processing

Figure 1A presents a schematic diagram of the developed PA imaging system, based on previous studies.[13,24] As the incident pulsed light beam source, a Q-switched Nd:YAG laser (Continuum Surelite II-10; Continuum, Santa Clara, CA, USA) with selective wavelengths of 532 nm and 1064 nm, a pulse width of 6 ns, and a repetition rate of 10 Hz was employed for this study. The laser beam diameter was measured to be approximately 7 mm.

This pulsed beam was elevated to a certain height with a right-angle prism and multiple mirror assemblies. A part of this beam was divided with a beam splitter and fed to a photodetector, which was employed to trigger the 200 MHz digital storage oscilloscope (DSO) (TDS 2024B; Tektronix, Beaverton, OR, USA). The remaining beam was reflected downwards with a controlled mirror (Fig. 1A). In order to increase the resolution of the PA imaging measurement, the beam diameter was decreased to 1 mm with a pinhole arrangement. At this stage, the effective maximum working beam density was maintained at 17 mJ/cm^2, which was lower than the safety limit of 20 mJ/cm^2 set by the American National Standards Institute (ANSI).[35]

The tooth sample was mounted on a holder and was placed inside a distilled water tank. This entire assembly was placed over a computer-controlled motorized X-Y translation stage MTS50-Z8 (Thorlabs Inc., Newton, NJ, USA). The PA signals were acquired by employing an immersion-type ultrasonic transducer V310-N-SU (Olympus, Waltham, MA, USA) with a center frequency of 5 MHz. The transducer was partially immersed into the water

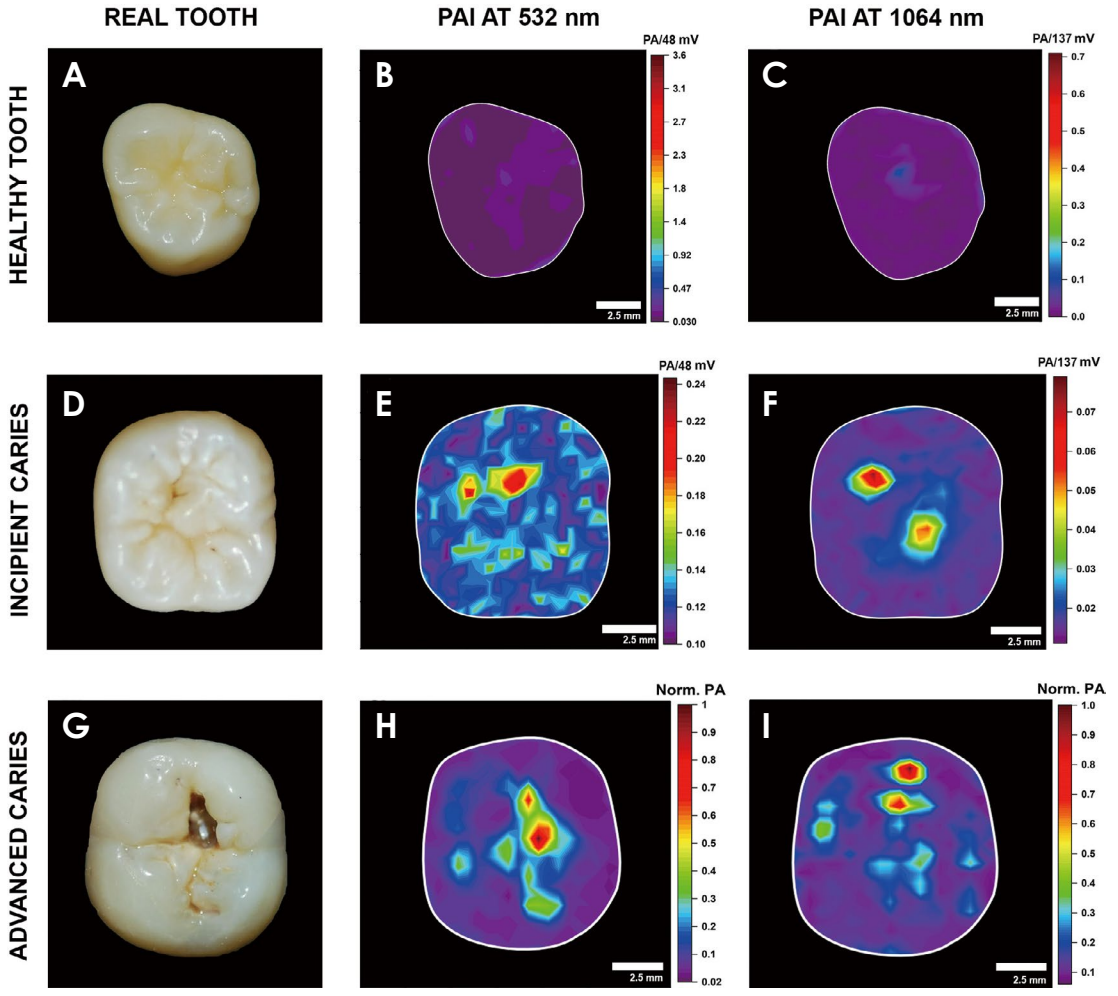

Fig. 2. Photoacoustic (PA) images of sound and carious teeth at 532 nm and 1064 nm with a 5-MHz photoacoustic detector. The rows represent the sound tooth (A-C); incipient caries (D-F); and advanced caries (G-I) groups. From the left to the right, the first column shows the photographic image of the representative samples, and the second and third columns show the corresponding PA images at 532 nm and 1064 nm, respectively. PAI: photoacoustic imaging.

pointing at the laser beam-tooth interface at 45° for optimal acoustic coupling with the sample. For depth measurements, the PA detector was placed on the tooth side and moved vertically from top to bottom with a computer-controlled Y-axis translation stage. To achieve a significant PA signal for imaging, a broadband signal amplifier was constructed and used to enhance the transducer output signal, which was finally fed to the DSO channel 1 (CH1).

For image reconstruction, the translation stages and DSO were interfaced with a custom-build LabVIEW program (National Instruments, Austin, TX, USA), as shown in Figure 1B. The X and Y stages were translated at 0.5-mm steps and PA data from the top surface of the tooth sample were recorded with CH1. The PA voltage signal in CH1 was averaged 16 times in order to remove the noise and the recorded peak-to-peak signal amplitude for every translation was fed into a 2D-array dataset in the program. Finally, the 2D dataset was used by the program to generate a color map contour plot of the respective sample automatically.

Results

With this automated PA imaging system, en-face images and depth measurements were obtained at pulse excitation wavelengths of both 532 nm and 1064 nm. Figure 2 shows an example of the PA imaging results for excitation at 532 nm and 1064 nm for a sound tooth, as well as teeth with incipient and advanced caries. Figure 3 also shows the radiographic and OCT results.

PA images of all teeth were acquired and the background noise was filtered out. A solid white outline was manually constructed in all PA images in order to mimic the respec-

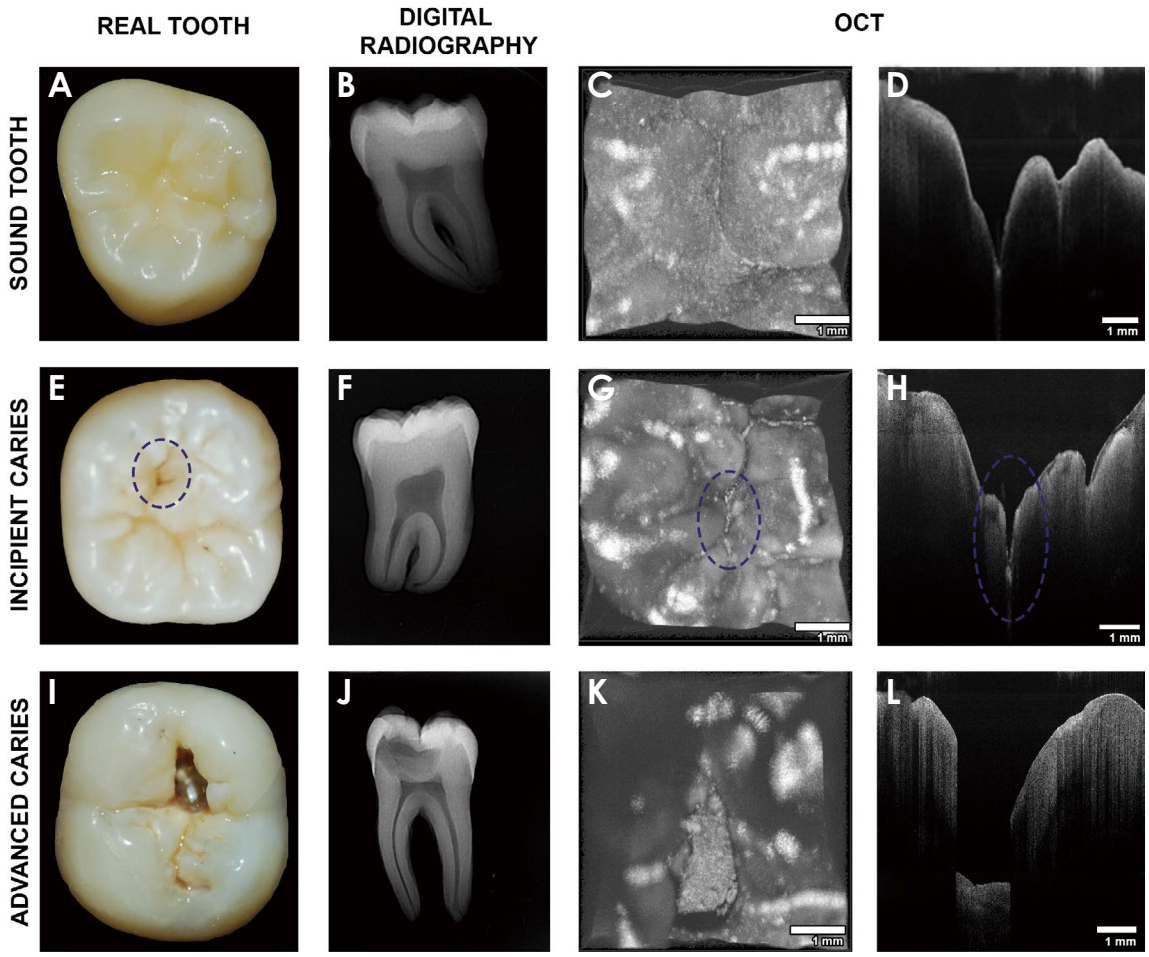

Fig. 3. Clinical, radiographic, 2-dimensional cross-sectional scans and 3-dimensional volumetric optical coherence tomographic (OCT) images of samples. Row A-D shows the clinical appearance of the sound tooth (A), digital radiography (B), volumetric OCT (C), and OCT cross-sectional view. Row E-H shows the equivalent results for the tooth with incipient caries, wherein the regions of interest are indicated by a dashed circle, depicting the clinical appearance (E), digital radiography (F), volumetric OCT (G), and OCT cross-sectional view (H). Similarly, row I-L shows the results for advanced caries; the clinical appearance is seen in (I), digital radiography in (J), volumetric OCT in (K), and the OCT cross-sectional view in (L).

tive tooth shape.

The color map contour PA images for all teeth with 532-nm excitation are plotted in Figures 2B, E, and H. To understand the effect of caries density on the PA signal, the PA imaging data for the entire sample was normalized to the maximum PA voltage signal of the carious sample. The PA imaging contour of the sound tooth showed no change of the photoacoustic signal throughout the entire tooth surface, indicating the absence of dental caries. However, the incipient caries PA imaging, as presented in Figure 2E, showed a significant amount of scattered PA signals, shown as red in the false color scale. Likewise, the PA imaging contour in Figure 2H shows a highly dense photoacoustic signal, confirming the presence of extensive dental caries in the tooth sample. The maximum amount of the normalized PA signal was defined as 1, corresponding to the maximum value of the PA voltage (48 mV) in this advanced caries sample. The normalization formula was therefore "PA/48 mV" (Figs. 2B, E, and H).

Similarly, PA imaging contour plots of all samples under an excitation wavelength of 1064 nm are shown in Figures 2C, F, and I. The sound tooth showed negligible photoacoustic effects, and hence the PA imaging contour was smooth throughout the surface (Fig. 2C). However, the PA imaging contour presented in Figure 2F showed 2 significant photoacoustic signals, suggesting the presence of 2 incipient caries on the tooth surface. The PA image for the tooth with advanced caries, presented in Figure 2I, clearly showed a high PA signal in the carious region, closely corresponding to the actual photograph of the tooth in Figure

2G. The highest normalized PA intensity for the caries was defined as 1, corresponding to the maximum PA signal voltage in this sample (137 mV). The normalization formula was therefore "PA/137 mV" (Figs. 2C, F, and I).

For completeness and comparison with the PA imaging, radiographic and OCT images from the same teeth were obtained, as they are well-established clinical (radiographic) and laboratory (OCT) methods for caries diagnostics, as described in previous studies.[11,12,36] The results are shown in Figure 3, which repeats the photographs of the sound, incipient, and advanced caries samples (Figs. 3A, E, and I, respectively) from Figure 2 (for ease of comparison by the reader) and presents them together with their corresponding radiographs (Figs. 3B, F, and J), volumetric OCT images (Figs. 3C, G, and K), and 2D OCT images (Figs. 3D, H, and L). As can be seen, radiography did not show any information on incipient caries (Fig. 3F). However, by comparing the OCT images, it is possible to observe the difference in the sulcus area of the demineralized sample (dashed circular area in Fig. 3G), which is also confirmed by the 2D OCT image (dashed circular area in Fig. 3H).

The OCT volumetric reconstruction of OCT images faithfully reproduced the photographed images, clearly identifying the ROI that was also verified by the PA imaging system. The unhealthy tissues are indicated in both the 3D OCT volumetric reconstructions (Figs. 3G and K) and the 2D OCT images (Figs. 3H and L). OCT was used here to confirm the PA imaging and can be considered the gold standard in this experiment.

The presence of dental caries in a tooth can also be quantified by calculating the contrast of the carious region obtained from various imaging tools, as shown in Figures 2 and 3. The image contrast can be evaluated using the well-known Weber contrast (W) formula, defined as:[37]

$$W = \frac{I_c - I_s}{I_s} \quad (1)$$

Where I_c and I_s are the luminance of the carious tissue and the sound area of the tooth, respectively. The calculated Weber contrast values for dental caries obtained from different imaging tools are shown in Table 1. It is evident from Table 1 that the incipient caries sample showed a significant amount of Weber contrast from the different imaging tools. It is worth noting here that digital radiography failed to detect any incipient carious tissues and therefore showed no Weber contrast, and contrast calculation for the healthy tooth was not possible due to the absence of caries. Among all the imaging techniques, PA imaging proved to be the best tool for incipient caries detection, as the Weber contrast values were 0.92 (for 532-nm excitation) and 4.16 (for 1064-nm excitation), considerably exceeding the values obtained with other imaging tools.

Table 1. Weber contrast values for dental caries obtained from different imaging tools

Imaging tools		Healthy tooth	Incipient caries	Advanced caries
Photographic image		–	0.50	1.56
Digital radiography		–	–	0.52
OCT (cross-section)		–	0.14	0.54
PA imaging	532 nm	–	0.92	11.03
	1064 nm	–	4.16	8.0

OCT: optical coherence tomography, PA: photoacoustic

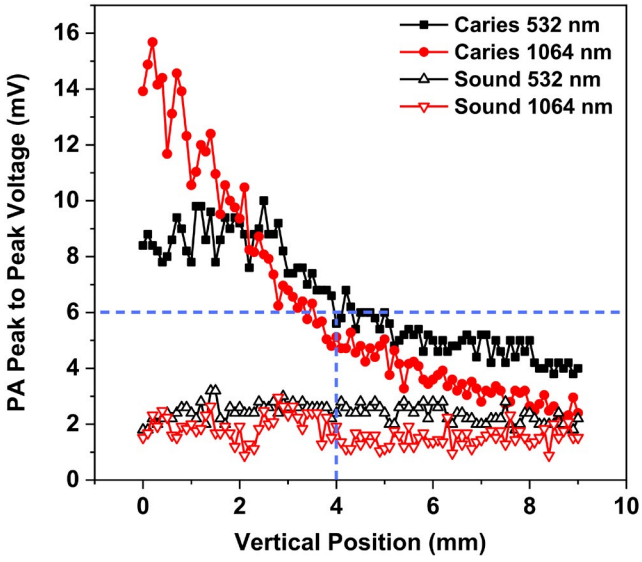

Fig. 4. Peak to peak voltage for the depth of the photoacoustic signal in a tooth with incipient caries (as shown by a dashed circle of interest in Figure 3G) with the laser beam directed at the lesion areas (closed black and red symbols) and a sound area (open black and red symbols) at laser wavelengths of 532 nm and 1064 nm.

The effectiveness of the photoacoustic technique to measure dental caries was confirmed and the experiment was repeated for 5 different tooth samples of each type; however, the data shown are representative of all other samples.

An important result is shown in Figure 4 regarding the depth at which the PA signal can be detected. When exciting the samples on the occlusal surface, exactly on the previously detected incipient caries area (as shown by a dashed circle of interest in Figure 3G), the PA detector was placed laterally to the long axis of the tooth while the detector

was displaced, and data were simultaneously acquired. In this way, it was possible to capture the PA intensity signal inside the sample. In Figure 4, the vertical position (mm) scaled up to 10 mm in the x-axis signifies the depth of the tooth sample from the top incipient carious surface (0 mm). As can be seen, for the sound tooth, a very small signal was detected for both wavelengths (above the noise floor), whereas when the light was incident on the carious region, the PA signal from wavelengths of either 532 nm or 1064 nm was clearly detected as a notable difference. PA signal intensities 40% above the noise floor were detected for both 532 nm and 1064 nm at a 4-mm depth, as indicated by the horizontal and vertical dotted lines in Figure 4.

Discussion

In this study, a new automated PA imaging system was developed, which can capture the PA imaging contour of teeth samples with non-ionizing laser excitation under a dual-wavelength source and a ultrasonic detector for acoustic detection of the generated PA signal. The developed PA imaging system involves automated XY scanning of the tooth surface and real-time data acquisition of the PA signals.

The amount of the PA signal is directly proportional to the light absorbed by the tissue;[38] thus, there is an evident link between the enhancement of PA signal voltage with the amount of dental caries. This result also confirms the efficiency of the PA imaging system, as every tooth showed a consistent rise of the PA signal depending on its condition. A notable advantage of PA detection is that it only relies on absorption, and light scattering does not affect the results. The PA imaging system described herein effectively detected incipient caries, which are difficult to identify with visual inspection or even radiography.

In examinations of the tooth face, the results clearly identified the presence of carious tissue at both wavelengths employed, and the images shown in Figure 2 were automatically obtained. The acquisition rate was limited by the 10-Hz repetition rate of the system, leading to an acquisition time of several minutes, which is not recommended for clinical applications. This technical limitation can be overcome by using kHz repetition rate sources, including light-emitting diode (LED) - based sources.[39]

An important result is that PA signals due to caries were detected down to a 4-mm depth. This finding implies that hidden caries in the enamel (typically 1-2 mm before reaching the dentin) can be easily detected. The spatial resolution of the system could be improved by using acoustic detectors with higher frequencies. By transforming this PA imaging system into a PA tomography system, a 3D image could be provided. The system could also be used to identify occlusal caries.

In this work, PA imaging experiments were performed at both visible (532 nm) and infrared (1064 nm) wavelengths. The results in Figure 2 and Figure 4 show that the PA signals from carious tissues could be acquired at excitation wavelengths of both 532 nm and 1064 nm. For the incipient carious sample excited with 1064-nm light, the obtained PA image was free from noise, and the carious area in Figure 2F closely follows the real image of the incipient carious region in Figure 2D. Moreover, the Weber contrast for the incipient carious tooth excited at 1064 nm was 4.16, or ~4.5 times higher than the contrast value obtained with 532 nm excitation. This result can also be validated by Figure 4, where the maximum intensity of the carious PA signal excited at 1064 nm is shown to be ~2 times higher than that obtained at 532 nm. The depth profile of the carious PA signal excited with light at a wavelength of 1064 nm was exponential with minimum fluctuations. Such results validate the use of a near-infrared light source for efficient PA imaging - based diagnoses.

For real-life clinical applications, only a single excitation is needed, and hence near-infrared wavelength excitation is mostly recommended for deep tissue imaging. Moreover, the use of near-infrared excitation opens up new possibilities for future optical fiber - guided flexible PA imaging systems, since at this wavelength the optical loss in the fiber is minimized compared to the loss of visible light.

These results demonstrate the feasibility of PA imaging detection of carious lesions in the early stages of dental disease. The results are consistent with those obtained by previous studies that used PA imaging systems to investigate early dental caries.[13,24,26,27] The PA imaging system presented in this research is fully automated, and real-life clinical applications with a handheld integrated PA system capable of fitting into the oral cavity can be pursued by following the technological developments reported in other studies.[40,41]

The results presented here are promising and corroborate that PA imaging can be applied as a diagnostic tool in caries research. New studies should focus on developing a clinical model of PA imaging applications in dentistry, including soft tissues. The use of LEDs instead of lasers will make PA imaging systems more flexible and user-friendly, together with detector miniaturization, which is already technologically feasible.

Conflicts of Interest: None

References

1. Cury JA, Tenuta LM. Enamel remineralization: controlling the caries disease or treating early caries lesions? Braz Oral Res 2009; 23 Suppl 1: 23-30.
2. Amaechi BT. Emerging technologies for diagnosis of dental caries: the road so far. J Appl Phys 2009; 105: 102047.
3. Melo M, Pascual A, Camps I, Del Campo Á, Ata-Ali J. Caries diagnosis using light fluorescence devices in comparison with traditional visual and tactile evaluation: a prospective study in 152 patients. Odontology 2017; 105: 283-90.
4. da Silva Neto JM, dos Santos RL, Sampaio MC, Sampaio FC, Passos IA. Radiographic diagnosis of incipient proximal caries: an ex-vivo study. Braz Dent J 2008; 19: 97-102.
5. Pitts NB, Zero DT, Marsh PD, Ekstrand K, Weintraub JA, Ramos-Gomez F, et al. Dental caries. Nat Rev Dis Primers 2017; 3: 17030.
6. Abogazalah N, Eckert GJ, Ando M. In vitro visual and visible light transillumination methods for detection of natural non-cavitated approximal caries. Clin Oral Investig 2019; 23: 1287-94.
7. Melo M, Pascual A, Camps I, Ata-Ali F, Ata-Ali J. Combined near-infrarred light transillumination and direct digital radiography increases diagnostic in approximal caries. Sci Rep 2019; 9: 14224.
8. Jung EH, Lee ES, Jung HI, Kang SM, de Josselin de Jong E, Kim BI. Development of a fluorescence-image scoring system for assessing noncavitated occlusal caries. Photodiagnosis Photodyn Ther 2018; 21: 36-42.
9. Felix Gomez G, Eckert GJ, Ferreira Zandona A. Orange/red fluorescence of active caries by retrospective quantitative light-induced fluorescence image analysis. Caries Res 2016; 50: 295-302.
10. Fried D, Staninec M, Darling CL, Chan KH, Pelzner RB. Clinical monitoring of early caries lesions using cross polarization optical coherence tomography. Proc SPIE Int Soc Opt Eng 2013; 8566: 856604.
11. Freitas AZ, Zezell DM, Vieira ND Jr, Ribeiro AC, Gomes AS. Imaging carious human dental tissue with optical coherence tomography. J Appl Phys 2006; 99: 024906.
12. Maia AM, de Freitas AZ, de L Campello S, Gomes AS, Karlsson L. Evaluation of dental enamel caries assessment using quantitative light induced fluorescence and optical coherence tomography. J Biophotonics 2016; 9: 596-602.
13. Cheng R, Shao J, Gao X, Tao C, Ge J, Liu X. Noninvasive assessment of early dental lesion using a dual-contrast photoacoustic tomography. Sci Rep 2016; 6: 21798.
14. Bell AG. Selenium and the photophone. Nature 1880; 22: 500-3.
15. Bell AG. The production of sound by radiant energy. Science 1881; 2: 242-53.
16. Tyndall J. Action of an intermittent beam of radiant heat upon gaseous matter. Science 1881; 2: 110-4.
17. Röntgen WC. On tones produced by the intermittent irradiation of a gas. London Edinburgh Dublin Philos Mag J Sci 1881; 11: 308-11.
18. Hordvik A, Schlossberg H. Photoacoustic technique for determining optical absorption coefficients in solids. Appl Opt 1977; 16: 101-7.
19. Tam AC. Applications of photoacoustic sensing techniques. Rev Mod Phys 1986; 58: 381-431.
20. Xia J, Yao J, Wang LV. Photoacoustic tomography: principles and advances. Electromagn Waves (Camb) 2014; 147: 1-22.
21. Li T, Dewhurst RJ. Photoacoustic imaging in both soft and hard biological tissue. J Phys Conf Ser 2010; 214: 012028.
22. Li L, Lin L, Wang LV. Multiscale photoacoustic tomography. Opt Photonics News 2018; 29: 32-9.
23. Fu Q, Zhu R, Song J, Yang H, Chen X. Photoacoustic imaging: contrast agents and their biomedical applications. Adv Mater 2019; 31: e1805875.
24. Kim K, Witte R, Koh I, Ashkenazi S, O'Donnell M. Early detection of dental caries using photoacoustics. In: Oraevsky AA, Wang, LV, editors. Photons plus ultrasound: imaging and sensing 2006: Proceedings of the Seventh Conference on Biomedical Thermoacoustics, Optoacoustics, and Acousto-optics; 2006 Jan 22-26; San Jose, CA, USA. Bellingham: SPIE; 2006. 60860G.
25. Rao B, Cai X, Favazza C, Yao J, Li L, Duong S, et al. Photoacoustic microscopy of human teeth. In: Rechmann P, Fried D, editors. Lasers in dentistry XVII: Proceedings of SPIE 7884; 2011 Jan 23; San Francisco, CA, USA. Bellingham: SPIE; 2011. 78840U
26. Koyama T, Kakino S, Matsuura Y. A feasibility study of photoacoustic detection of hidden dental caries using a fiber-based imaging system. Appl Sci 2018; 8: 621.
27. Hughes DA, Sampathkumar A, Longbottom C, Kirk KJ. Imaging and detection of early stage dental caries with an all-optical photoacoustic microscope. J Phys Conf Ser 2015; 581: 012002.
28. Lin CY, Chen F, Hariri A, Chen CJ, Wilder-Smith P, Takesh T, et al. Photoacoustic imaging for noninvasive periodontal probing depth measurements. J Dent Res 2018; 97: 23-30.
29. Moore C, Bai Y, Hariri A, Sanchez JB, Lin CY, Koka S, et al. Photoacoustic imaging for monitoring periodontal health: a first human study. Photoacoustics 2018; 12: 67-74.
30. Lee D, Park S, Kim C. Dual-modal photoacoustic and ultrasound imaging of dental implants. In: Oraevsky AA, Wang LV, editors. Photons Plus Ultrasound: Imaging and Sensing 2018: Proceedings of SPIE 10494; 2018 Jan 28-Feb 1; San Francisco, CA, USA. Bellingham: SPIE; 2018. 104940B.
31. Yamada A, Kakino S, Matsuura Y. Detection of photoacoustic signals from blood in dental pulp. Opt Photonics J 2016; 6: 229-36.
32. Ekstrand KR, Gimenez T, Ferreira FR, Mendes FM, Braga MM. The International Caries Detection and Assessment System - ICDAS: a systematic review. Caries Res 2018; 5: 406-19.
33. Huang D, Swanson EA, Lin CP, Schuman JS, Stinson WG, Chang W, et al. Optical coherence tomography. Science 1991; 254: 1178-81.
34. Fujimoto JG. Optical coherence tomography for ultrahigh resolution in vivo imaging. Nat Biotechnol 2003; 21: 1361-7.
35. Laser Institute of America [Internet]. Orlando: ANSI Z136 Standards [cited 2020 Sep 15]. Available from: https://www.lia.org/resources/laser-safety-information/laser-safety-standards/ansi-z136-standards.
36. Hsieh YS, Ho YC, Lee SY, Chuang CC, Tsai JC, Lin KF, et al. Dental optical coherence tomography. Sensors (Basel) 2013; 13: 8928-49.

37. Yu L, Sun J, Lv X, Feng Q, He H, Zhang B, et al. High-contrast photoacoustic imaging through scattering media using correlation detection of adaptive time window. Sci Rep 2019; 9: 17262.
38. Beard P. Biomedical photoacoustic imaging. Interface Focus 2011; 1: 602-31.
39. Zhu Y, Xu G, Yuan J, Jo J, Gandikota G, Demirci H, et al. Light emitting diodes based photoacoustic imaging and potential clinical applications. Sci Rep 2018; 8: 9885.
40. Colchester RJ, Zhang EZ, Mosse CA, Beard PC, Papakonstantinou I, Desjardins AE. Broadband miniature optical ultrasound probe for high resolution vascular tissue imaging. Biomed Opt Express 2015; 6: 1502-11.
41. Cao Y, Jin W, Ho HL, Ma J. Miniature fiber-tip photoacoustic spectrometer for trace gas detection. Opt Lett 2013; 38: 434-6.